MEMS Magnetic Sensor in Standard CMOS

Beverley Eyre and Linda Miller

Jet Propulsion Laboratory, California Institute of Technology, Pasadena

Kristofer S. J. Pister

University of California, Berkeley

Abstract. A novel micromechanical magnetic sensor has been built and tested. The field is detected by measuring the vibration amplitude of a mechanical Lorentz force oscillator. This device is made from a standard two micron CMOS fabrication process with a post-processing etch step to undercut and release the sensor. When operated at the resonant frequency of the mechanical system, a sensitivity of 20 μVolts per Gauss was measured.

1. Introduction

1.1 Background

Magnetic sensors using the Hall effect as their principle of transduction are commonly made in standard CMOS and have reached a high level of predictable performance and utility [*Baltes et al.*, 1986]. However, semiconductor magnetic sensors based in silicon may have intrinsic limits to their sensitivity and resolution which may limit future gains in performance [*Chovet et al.*, 1990]. With this in mind magnetic sensors of different types are being explored with the hopes of expanding the range of applications as well as the performance of CMOS-based magnetic sensors. The work described here is one such application and is based on a micro electromechanical systems (MEMS) approach.

1.2 Micro-coil Based Magnetic Sensors

Many types of sensors have been fabricated in standard CMOS using the strategies and techniques of micro-machining [*Baltes*, 1993]. Magnetic sensors using metal loops on an undercut plate have also been fabricated in previous work, both in custom processes [*Kadar et al.*, 1994], and in standard CMOS [*Shen and Allegretto*, 1996]. Micro-coils have been used to generate and sense high frequency magnetic fields [*Hirota et al.*, 1993; *Eyre et al.*, 1995] with, in some respects, superior performance to traditional magnetic sensors, especially in the area of temperature response. Low frequency or DC magnetic fields can also be sensed by placing within them a micro-coil and utilizing the Lorentz force. Using a custom micro-machining process Kadar et al. [1994] introduced a resonant magnetic sensor based on this principle, where displacement was detected via capacitive sensing. Our approach is similar to theirs in the design of the moving plate, however in our device sensing is done with polysilicon piezoresistors.

2. Description

The sensor was fabricated using the Orbit two-micron N-well process through the MOSIS service. After fabrication an unmasked etch using XeF_2 [*Chang et al.*, 1995] is performed in order to free the mechanical system and allow it to rotate.

The sensor consists of an oxide plate held suspended over a cavity etched in the silicon substrate by two sets of support beams (Figure 1). The support beams jut from the edges of the etched cavity near the center of the plates' long side. At the end of these beams, and perpendicular to them, are 'L' shaped beams which travel the length of the plate's long side and connect to the suspended plate near its end.

The 'L' beams on one side of the plate contain two polysilicon piezoresistors which act as the active pair of a set of four resistors forming a Wheatstone bridge (Figure 2). When the resistors are strained by the bending of the beams the Wheatstone bridge transduces a change in resistance into a change in voltage. This voltage signal can then be sent to electronics for processing.

The set of beams on the other side of the oxide plate are used to bring a metal loop onto and off of the plate. This 'current loop' encircles the plate around its perimeter. During operation a sinusoidal signal is sent through the current loop whose function is to interact with the magnetic field and produce a force which acts on the plate.

3. Analysis

The sensor is placed in a transverse magnetic field while a sinusoidal current is excited within the loop. This will generate a force which tends to push up on one side of the plate and down on the other (fig. 3). This force is given by:

$$F_s = I_L L_s B_x \tag{1}$$

where I_L is the loop current, B_x is the magnetic field across the plate, and L_s is the length of the side perpendicular to the magnetic field. F_s is the force on only one side of the plate.

The plate will rotate about an axis running through the support beams and create a strain in the piezoresistors. For a small rotation, the total moment experienced at the base of the bending beams will be:

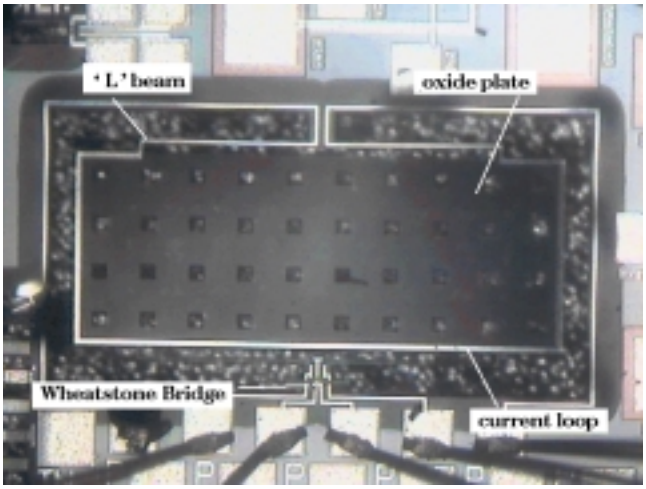

Figure 1. Top view photomicrograph of sensor. An oxide plate is suspended over an etched cavity in a silicon substrate held by torsional support beams and 'L' shaped beams.

Science Closure and Enabling Technologies for Constellation Class Missions, edited by V. Angelopoulos and P. V. Panetta, pp. 99-102 , UC Berkeley, Calif., 1998.

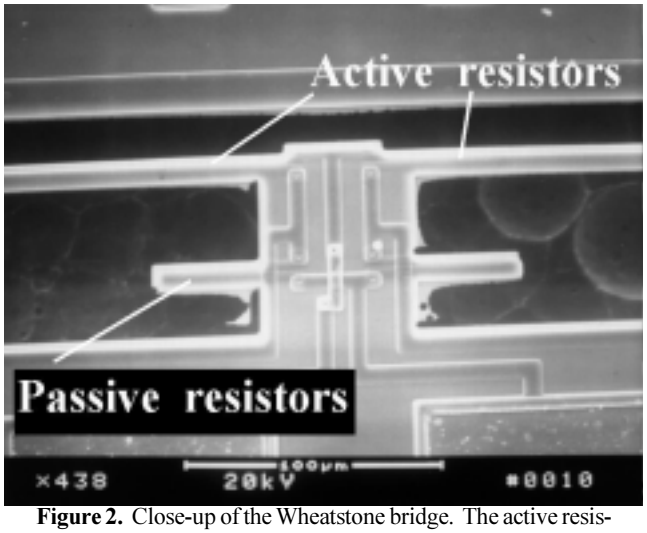

Figure 2. Close-up of the Wheatstone bridge. The active resistors are contained within the 'L' beams and are strained when the plate rotates. The passive resistors are designed to be in close proximity to the active resistors in order to share the same environmental factors, such as temperature, which can change the value of the polysilicon resistors.

$$M = 2F_s L_{ma} \tag{2}$$

where L_{ma} is the length from the end of the plate to the base of the piezoresistors. The moment is proportional to the area of the plate $A_p = 2L_s L_{ma}$.

The strain felt by the piezoresistors is:

$$\varepsilon = \frac{M_z}{EI_b} \tag{3}$$

where z is the distance from the neutral axis of the bending beam to the polysilicon piezoresistors and EI_b is the total flexural rigidity of all four beams. These resistors are two of the set of four configured in the Wheatstone bridge (Figure 2). The change in resistance is related to the strain by the gauge factor G, defined by:

$$\frac{\Delta R}{R} = G\varepsilon \tag{4}$$

For n-type polysilicon G is $\cong -20$ [French and Evans, 1985].

The change in resistance of the strained piezoresistors becomes a change in voltage within the Wheatstone bridge and thus the magnetic field is transduced into a voltage. For a bridge with two active resistors:

$$\frac{\Delta V}{V} = \frac{\Delta R}{2R} \tag{5}$$

This voltage can be used as the signal input to on-chip signal processing circuits in the creation of a 'smart' sensor. This step of integration has not yet been taken with this sensor, though similar systems have been demonstrated in the same process [*Lin et al.*, 1996].

From this analysis we get the expression for the sensitivity of the sensor:

$$S = \frac{\Delta V}{\Delta B} = \frac{zGI_L VA_p}{EI_b} \tag{6}$$

When running the sensor at the resonant frequency of the mechani-

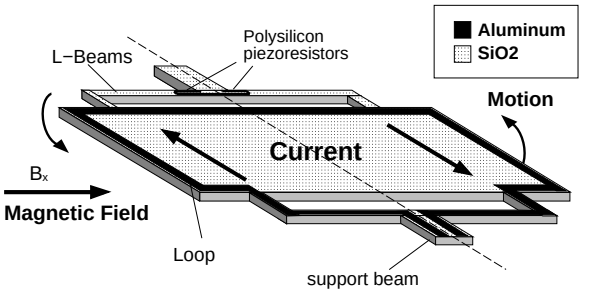

Figure 3. Schematic showing the operation of the sensor. The current loop is excited by a sinusoidal signal while the sensor is placed in a transverse magnetic field. Since the direction of the current on one side of the plate is the reverse of the current on the other, with respect to the magnetic field, a force will be generated pushing the plate up one side and down on the other. Because the signal is a sinusoid, the plate will rock with a see-saw motion.

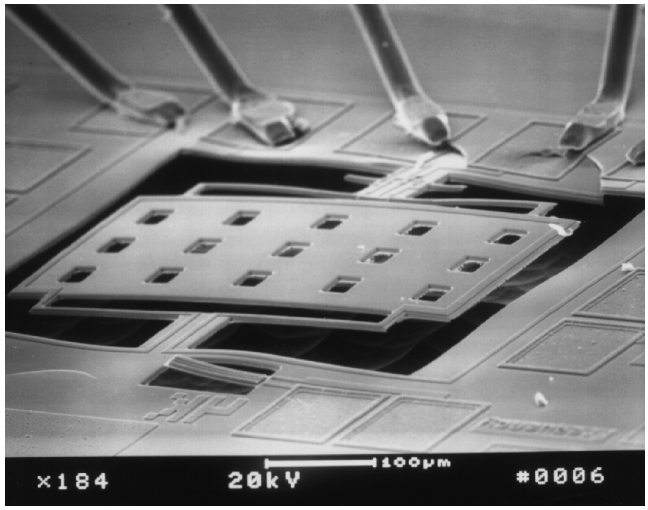

Figure 4. SEM of a smaller version of the resonant mechanical sensor. The oxide is seen to have a small stress gradient. The holes on the plate are for the purpose of having a faster etch time. This device was released using 50 one minute pulses of xenon difluoride gas at room temperature. The etch pressure was $\cong$ 20 *mTorr*.

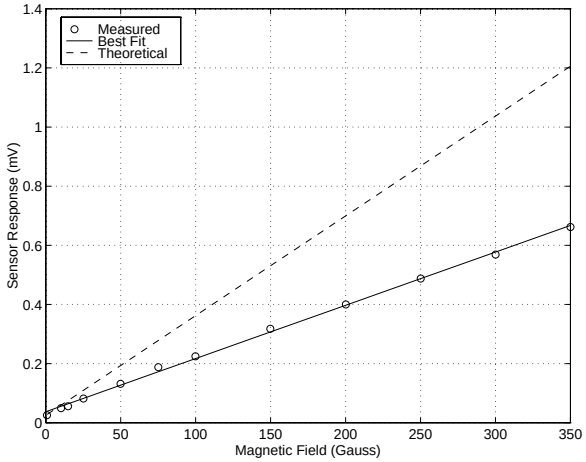

Figure 5. The sensitivity of the sensor is plotted here. These tests were run at low power for the sake of keeping the sensor within safe operating ranges, and were for the purpose of testing the accuracy of the model. The sensitivity of the sensor is a function of Q, the plate area, the 'pseudo' power (loop current × Wheatstone bridge voltage) and a constant. There is a slight offset voltage corresponding to $\cong$ 15 *Gauss*.

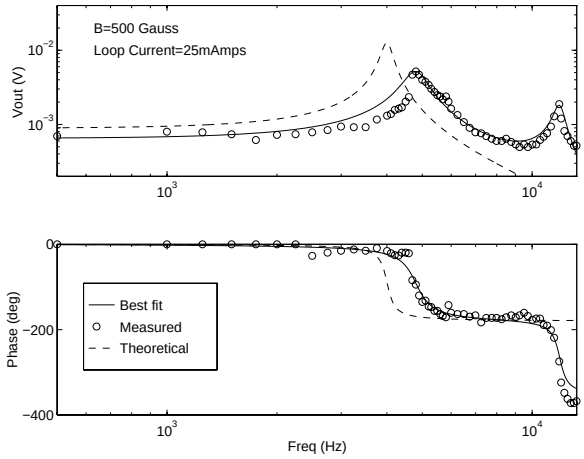

Figure 6. Bode plot of first generation device. This device shows a resonant peak near the predicted value, and an additional peak at roughly twice that value. The Q of this device is $\cong$ 10 at the first resonant frequency. Testing at low pressure indicates that the damping is mostly internal and due to the aluminum traces that travel onto and off the plate via the 'L' beams.

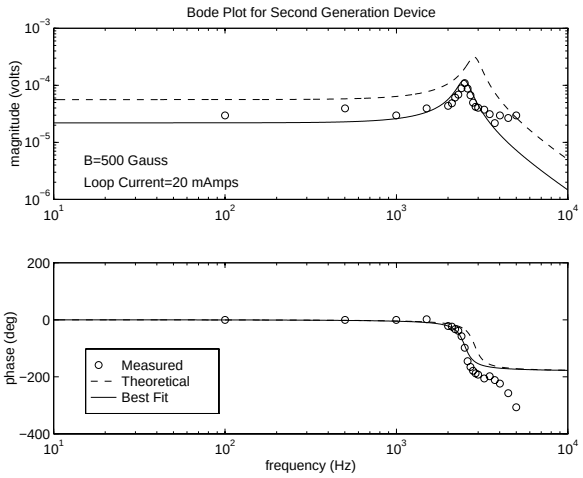

Figure 7. Bode plot of second generation device. This version of the sensor had thicker 'L' beams than the first generation. This was to increase the yield of the devices which was low at first due to cracking of the beams and consequent etching of the polysilicon piezoresistors. This widening of the beams may account for the slight lessening of the Q.

cal system the sensitivity is multiplied by the quality factor Q.

The sensitivity can be expressed as a function of four factors: 1) the Q of the sensor; 2) C, a constant made up of process parameters, physical constants, and the flexural rigidity of the beams; 3) A, the area of the plate; 4) P, a term with units of power made up of the product of the Wheatstone bridge voltage and the loop current.

$$S = QCAP \tag{7}$$

It should be noted here that the dynamic range of the sensor can be tuned via on-chip electronics by altering one of the components of the power term. This would permit the sensor to have a large dynamic range. The resonant frequency of the system can be approximated by:

$$\omega_0 = \sqrt{\frac{K}{m}} \tag{8}$$

where

$$K = \frac{Ea^3b}{4L_b^3} \tag{9}$$

is the spring constant of four beams, m is the mass of the plate-beam system, E is the Young's Modulus of the bending beams, L_b is the length of the bending beam, and a and b are the thickness and width of the beam, respectively.

4. Results and Discussion

Testing was performed by independently varying conditions of magnetic field strength, loop current and Wheatstone bridge voltage. Figure 5 plots the voltage output of the Wheatstone bridge as a function of magnetic field strength. There is an AC loop current of ten milliamps at 2.5 KHz, the mechanical resonant frequency of the plate-beam system, and a 1 Volt drop across the Wheatstone bridge. These values were chosen not to test the ultimate sensitivity of each device, but merely to compare the measured response to the theoretical model. For this reason they are well within the safe operating range of the devices.

The response is linear with a slight voltage offset. This offset corresponds to roughly fifteen Gauss. Figures 6 and 7 show the Bode plots of two generations of devices. While the DC level of the first generation seems closer to the theoretical model, the resonant frequency of the second generation is the more accurate. The first generation devices had a small yield due to the width of the 'L'beams, which cracked easily upon release. This was remedied in the second generation by making these beams wider.

The best fit curves are two and four pole systems respectively with the measured peak frequencies, DC level, and damping factor as input parameters. The theoretical curve is calculated from equations (6) and (8) and from the magnetic field, voltages, and currents used in the experiment. The damping factor used in this calculation was the one measured during testing.

Testing was performed to find the relation between Q and pressure. The results indicated that there was another source of damping in addition to viscous damping. This additional damping could be due to the aluminum traces that bring the current onto the loop and are within the 'L' beams. This would explain the smaller value for Q in the second generation where the aluminum traces were slightly wider than the first. This damping is dominant and consequently the Q increased only slightly at low pressure.

5. Conclusion

A new magnetic sensor in standard CMOS has been designed and tested. This sensor needs a post-fabrication etching step to undercut the sensor and allow it to rotate.

The response is shown to be linear within the range of magnetic fields tested. The frequency behavior shows a two pole response for the later generation and indicates that running the sensor at the resonant frequency of the system will result in the greatest output magnitude. Assuming thermal noise in the piezoresistors as the ultimate limitation of resolution for this sensor, this second generation device should be capable of measuring signals as small as 25 nTesla/ Hz. With future design improvements 1-10 nTesla/ Hz should be possible.

Acknowledgments. This work was supported by NSF under IRI-9321718, by DARPA, by the Directors Research and Development Fund of the Jet Propulsion Laboratory, California Institute of Technology, and by the National Aeronautics and Space Administration, Office of Space Sciences.

References

H. Baltes and R. Popovic, Integrated semiconductor magnetic field sensors, *Proc. IEEE*, *74(8)*, 1107-1132, 1986.

A. Chovet, et al., Comparison of noise properties of different magnetic-field semiconductor integrated sensors, *Sensors and Actuators*, Add(1-3):790-4, March 1990.

H.P. Baltes, CMOS as sensor technology, *Sensors and Actuators, A37-A38*, 51-56, June-August 1993.

Z. Kadar, et al., Integrated resonant magnetic-field sensor, *Sensors and Actuators*, *A41(1-3),* 66-69, April 1994.

B. Shen and W. Allegretto, CMOS micromachined cantileverin-cantilever devices with magnetic actuation, *IEEE Electron Device Letters, 17(7),* 372-374, July 1996.

T. Hirota, et al., Development of micro-coil sensor in standard CMOS, *SPIE Symposium on Micro-Machining and Micro-fabrication, 2642,* 183-191, Austin, TX, October 1995.

F. Chang, et al., Gas-phase silicon micro-machining with xenon difluoride, SPIE Symposium on Micro-machining and Micro-fabrication, *264f1*, 117-128, Austin, TX, October 1995.

P.J. French and A.G.R. Evans, Polycrystalline silicon strain sensors, *Sensors and Actuators, 8,* 219-225, 1985.

G. Lin, et al., Standard CMOS piezoresistive sensor to quantify heart cell contractile forces, *Proc. IEE Micro Mechanical Systems Workshop,* 150-155 p.p., San Diego, Feb 1996.

Beverly Eyre and Linda Miller, Jet Propulsion Laboratory, California Institute of Technology, Pasadena, CA 91109. (e-mail: fbeyre@mail1.jpl.nasa.gov, linda.m.miller@jpl.nasa.gov)

Kristofer S. J. Pister, University of California, Berkeley, CA 94720. (e-mail: pister@eecs.berkeley.edu)